Quantum Interference in Macroscopic Crystals of Nonmetallic Bi$_2$Se$_3$

J. G. Checkelsky,[1] Y. S. Hor,[2] M.-H. Liu,[1] D.-X. Qu,[1] R. J. Cava,[2] and N. P. Ong[1]

[1]*Department of Physics, Princeton University, Princeton, New Jersey 08544, USA*
[2]*Department of Chemistry, Princeton University, Princeton, New Jersey 08544, USA*

Photoemission experiments have shown that Bi$_2$Se$_3$ is a topological insulator. By controlled doping, we have obtained crystals of Bi$_2$Se$_3$ with nonmetallic conduction. At low temperatures, we uncover a novel type of magnetofingerprint signal which involves the spin degrees of freedom. Given the mm-sized crystals, the observed amplitude is 200–500$\times$ larger than expected from universal conductance fluctuations. The results point to very long phase-breaking lengths in an unusual conductance channel in these nonmetallic samples. We discuss the nature of the in-gap conducting states and their relation to the topological surface states.

A new class of insulators with nontrivial topological surface states has been predicted [1–5]. The surface states of these topological insulators are chiral, and protected from disorder by a large spin-orbit interaction that aligns the spin transverse to the wave vector. Angle-resolved photoemission spectroscopy (ARPES) has been used to detect these surface states (SS) in Bi$_{1-x}$Sb$_x$ [6]. The spin polarization of the SS in Sb was confirmed by spin-resolved ARPES [7]. More recently, ARPES experiments showed that Bi$_2$Se$_3$ [8,9] and Bi$_2$Te$_3$ [10] are the simplest topological insulators, with only a single Dirac surface state.

Because of its large band gap (300 mV), Bi$_2$Se$_3$ is a very attractive platform for exploring the transport properties of the topological states. However, as-grown crystals of Bi$_2$Se$_3$ invariably display a metallic resistivity profile, with the bulk chemical potential μ_b pinned to the conduction band. By chemical doping, we have obtained crystals of Bi$_2$Se$_3$ in which μ_b falls inside the gap. Although the residual conductance at low temperature T (0.3 K) appears to be still dominated by bulk conduction channels, we observe a novel type of conductance fluctuation phenomenon. In a swept magnetic field H, the fluctuations retrace reproducibly, analogous to the magnetofingerprint signal reminiscent of universal conductance fluctuations (UCF) [11]. However, the fingerprint signal here is observed in mm-sized bulk crystals rather than mesoscopic samples. Moreover, field-tilt experiments show that the carrier spin plays a role in generating the fluctuations. We discuss the highly unusual nature of the large magnetofingerprint signal and possible connections to the topologically protected surface states.

The ARPES results [8] reveal that Bi$_2$Se$_3$ has a single Dirac surface state (SS) that crosses the bulk energy gap [Fig. 1(a)]. In as-grown crystals, electrons donated by Se vacancies pin μ_b to the conduction-band (CB) edge. Recently, Hor *et al.* showed that doping with Ca converts the crystals to *p*-type conductors [12]. By tuning the Ca

content x in Ca$_x$Bi$_{2-x}$Se$_3$, we progressively shift μ_b from the CB to inside the gap, and then into the valence band (VB). Samples with μ_b in the CB or VB display Shubnikov–de Haas (SdH) oscillations which we have used to measure the caliper area $\mathcal{S}_F$ of the bulk Fermi surface (FS). The carrier sign was found by the thermopower and Hall effect. The index plots of the Landau levels
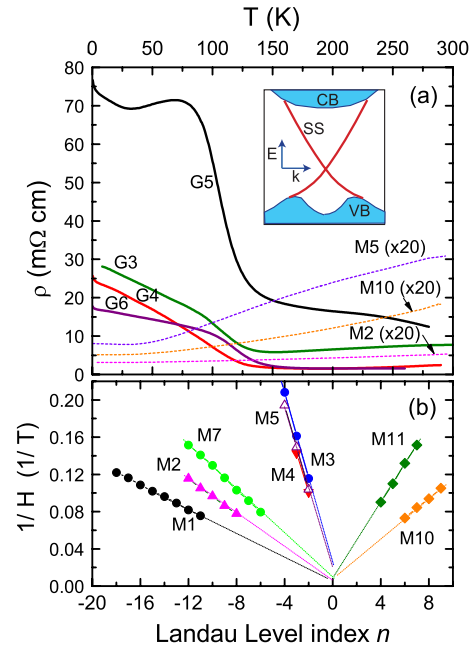

FIG. 1 (color online). (a) Resistivity ρ vs T in 4 samples (G3–G6) of Ca$_x$Bi$_{2-x}$Se$_3$ lightly doped with Ca to bring μ_b into the gap. Samples with μ_b not inside the gap (M2, M5, and M10) display a metallic T dependence (shown $\times$20). The inset is a sketch of the surface states [8] crossing the gap from the VB to the CB. (b) The LL index plot vs field minima in the SdH oscillations observed in 8 metallic samples (M1···M11). Negative (positive) index n represents the electron (hole) FS pocket. As μ_b is lowered from the CB to VB, the FS area $\mathcal{S}_F \sim$ 1/slope decreases before rising again.

[Fig. 1(b)] shows that $\mathcal{S}_F$ decreases (samples $M1 \rightarrow M3$) as μ_b enters the gap from the CB, and then increases as μ_b exits the gap and moves into the VB. The metallic profiles of ρ are shown in expanded scale in Fig. 1(a) ($M2$, $M5$, and $M10$). Using the changes in $\mathcal{S}_F$ to guide the doping, we have obtained nonmetallic crystals in a narrow doping window $0.002 < x < 0.0025$, with μ_b lying inside the energy gap. SdH oscillations are not resolved in any of the nonmetallic samples.

As plotted in Fig. 1(a), ρ of the nonmetallic crystals ($G3$–$G8$) undergoes an increase to very large values (20–100 mΩ cm) as T falls below 130 K. Below 20 K, ρ approaches saturation instead of diverging as in a semiconductor. Although the conductances G of the nonmetallic crystals are very poor (Table I), they are still 1000–8000× the universal conductance e^2/h (e is the charge and h is Planck's constant). As we will describe, draining away the high-mobility electrons in the CB uncovers a conductance channel of a highly unusual kind.

The magnetoresistance (MR) in sample $G4$, measured with $\mathbf{H} \parallel \hat{\mathbf{c}} \parallel \hat{\mathbf{z}}$ (with the current $\mathbf{I} \parallel \hat{\mathbf{x}}$), is displayed in Fig. 2(a) for $T = 0.3$–8 K. In each curve, the most prominent feature is the pronounced weak-field anomaly, which deepens to a sharp cusp at $H = 0$. Near the cusp, ρ vs H follows a logarithmic behavior extending over two decades in H at 0.3 K [Fig. 2(b)]. Moreover, at low T, large conductance fluctuations ($\sim 0.5\%\rho$) are apparent. The retraceability of the fluctuations versus H distinguishes them from random noise (the correlation function shown in panel (c) is discussed later).

Traces of the conductance fluctuations $\delta G(T, H) = G(T, H) - G_0(T, H)$, relative to the smoothed background $G_0(T, H)$, are displayed in Fig. 3 for three field orientations [$\mathbf{H} \parallel \hat{\mathbf{z}}$, $\mathbf{H} \parallel \hat{\mathbf{y}}$, and $\mathbf{H} \parallel \hat{\mathbf{x}}$ in panels (a), (b), and (c), respectively]. In each panel, we have emphasized the retraceability of $\delta G(T, H)$ by superposing the up- and downsweep curves at 0.3 K. Significantly, they remain large even with $\mathbf{H} \parallel \mathbf{I}$ [Fig. 3(c)]. We have followed the fluctuations to fields of 32 T in $G4$ and $G8$. The root-mean-square (rms)

amplitude is nearly unchanged between 4 and 32 T (by contrast, SdH amplitudes should grow exponentially). In all nonmetallic crystals studied at $T < 3$ K (Table I), the magnetofingerprint is present.

The existence of such large conductance fluctuations, with amplitudes $\pm 10 e^2/h$, is remarkable in a bulk mm-sized crystal ($2 \times 2 \times 0.05$ mm^3 for $G4$). Because magnetofingerprints imply field modulation of the interference between conductance contributions from many channels, it is natural to compare them with Aharanov-Bohm (AB) oscillations and UCF investigated in mesoscopic samples. However, we will argue that they belong in a new category.

To see this, we recall the main features of the AB oscillations and UCF. In mesoscopic, multiply connected samples (single loops or arrays of loops), two types of conductance oscillations are observed with periods in flux $\phi = h/2e$ and h/e, respectively. The former, called AAS oscillations [13,14], involves interference between a pair of time-reversed states that circumscribe a loop in opposite directions, and are observed only in very weak H (<100 Oe). The latter (AB oscillations), arising from interference between waves that traverse opposite arms of the loop, survive to very large H (>10 T). However, the AB oscillations do not ensemble average. When the sample size L exceeds the phase-breaking length $L_\phi \sim 1$ μm, the amplitudes decrease as $\sqrt{L_\phi/L}$ [15]. By contrast, the AAS
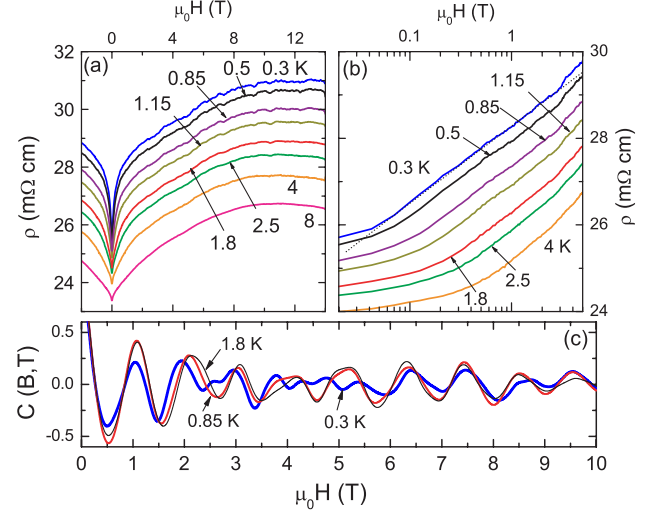

FIG. 2 (color online). Curves of ρ vs H in sample $G4$ at $0.3 < T < 8$ K. The curves are plotted vs H (panel a) and vs ln$H$ (b). The MR displays a sharp anomaly of amplitude 10%R in weak H. In addition, large conductance fluctuations of amplitude up to 0.5% are resolved. In panel (b), the plot of ρ vs log$H$ at 0.3 K shows that $\rho(H) \sim$ ln$H$ over two decades in H (dashed line). The slope is equivalent to dG/dln$H = 200$ e^2/h. The correlation function $\mathcal{C}(B, T)$ of the fingerprint signals ($\mathbf{H} \parallel \mathbf{z}$) is plotted in panel (c) for $T = 0.3$ K (bold curve), 0.85 K (medium), and 1.8 K (thin). $\mathcal{C}(B)$ oscillates vs H instead of decaying as a power law.

TABLE I. Sample parameters. c is the crystal thickness along $\mathbf{c}$. Values of G and rmsδG (in e^2/h) and ρ are measured at 0.3 K (except for $G3$, which was not cooled below 4 K). We define $A \equiv A_{orb} + A_{spin}$ [see Eq. (2)]. The crystals are of nominal size 2 mm $\times$ 2 mm $\times c$. The Hall density $n_H = 1/eR_H$ is inferred from the Hall coefficient R_H.

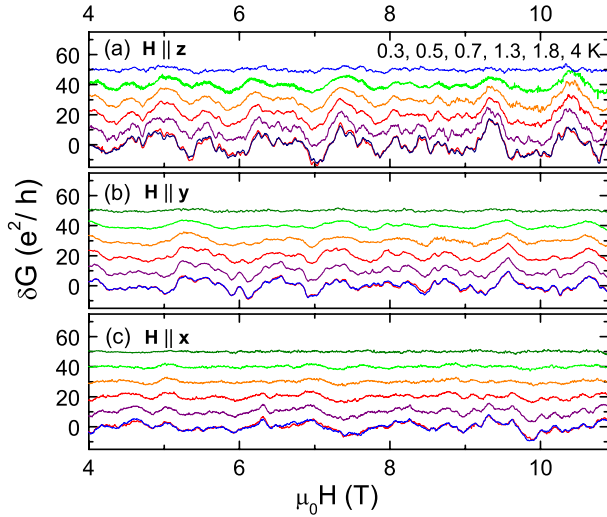| Units	ρ mΩ cm	c μm	G e^2/h	rmsδG e^2/h	A	n_H 10^{18} cm^{-3}
$G3$	30	50	$\cdots$	$\cdots$	$\cdots$	0.7
$G4$	15	50	8000	5.9	178	5
$G5$	76	80	1760	0.8	35	1
$G6$	18	50	7000	1	135	7
$G7$	16	25	4800	0.9	63	8
$G8$	25	10	1050	0.6	20	5

FIG. 3 (color online). Curves of the magnetofingerprint signal $\delta G(T, H)$ vs H in sample $G4$. The field **H** is aligned with $\hat{z}$ [in panel (a)], with $\hat{y}$ [in (b)], and with $\hat{x} \parallel \mathbf{I}$ [in (c)]. In each panel, curves are shown for five T between 0.3 and 4 K (in ascending order). For clarity, adjacent curves are displaced vertically by $10\ e^2/h$. At 0.3 K, both up-sweep and down-sweep traces are shown superposed to emphasize retraceability.

oscillations have been observed—with weak H—in giant arrays (10^6 loops) mm in size [16].

Apart from periodic oscillations, there exist weak, aperiodic fluctuations of the conductance G vs H (UCF) in simply connected mesoscopic samples [17,18]. For electrons undergoing quantum diffusion in a phase-coherent region ($L \sim L_\phi$), the fluctuations δG do not self-average. The rms value rms[δG] is $\sim e^2/h$ [11,19–21]. Modulation of the interference by H results in the magnetofingerprint trace. The amplitude of UCF is also sharply suppressed if L exceeds L_ϕ. In metals, the phase-coherent region is actually cut off by the thermal length $L_T = \sqrt{hD/k_B T}$, where D is the diffusion constant. As a result, UCF has been observed only in 1D (nanowires) and 2D systems (ultrathin films and semiconductor devices) in samples with $L \leq L_T \sim 1\ \mu$m [17,18]. Magnetofingerprint signals in large H have never been reported in mm-sized samples (in 2D or 3D).

Hence, at $T \sim 1$ K, both the AB oscillations and UCF, which persist to intense H, are confined to μm-sized samples, whereas the AAS oscillations may be observed in mm-sized periodic arrays, provided $H < \sim 200$ Oe. These comparisons show that the fingerprint signal in Bi_2Se_3 is difficult to account for in terms of AB or AAS oscillations or UCF. Specifically, with $D \sim 0.05\ \text{m}^2/\text{s}$, we find $L_T \sim 1.5\ \mu$m at 1 K. The measured volume in $G4$ ($2 \times 10^{-4}\ \text{cm}^3$) exceeds the phase-coherent volume L_T^3 by a factor of 6×10^7. By classical averaging, the UCF should be strongly suppressed. Quantitatively, the scaling of the variance of G with L is derived [11] as var[$G(L)$] $\sim (e^2/h)^2 (L_T/L)^{4-d}$, with d the dimension. This gives the

rms amplitude of UCF as 0.01–0.05 e^2/h, or 200–500 times weaker than depicted in Fig. 3.

Further insight into the fingerprint is obtained from its autocorrelation function

$$\mathcal{C}(B, T) = \frac{\langle \delta G(B', T) \delta G(B' + B, T) \rangle_{B'}}{\langle \delta G^2 \rangle}, \quad (1)$$

which measures how a particular peak of δG is correlated with peaks at other field values ($\langle \cdots \rangle_{B'}$ means averaging with respect to B', and $B = \mu_0 H$ with μ_0 the permeability). As calculated [11], $\mathcal{C}(B)$ for UCF should have a power-law decay $\sim B^{d-4}$.

In Fig. 2(c), we plot the correlation $\mathcal{C}(B, T)$ calculated from the results in Fig. 3(a). Instead of a power-law decay, $\mathcal{C}(B)$ is oscillatory, displaying ~ 9 periods with an average period $B_p \sim 1$ T. If we interpret our period B_p as a characteristic length $L_p \simeq \sqrt{\Phi_0/B_p} \simeq 640$ Å, the results suggest a characteristic area L_p^2 in the network of conduction paths.

The spin **s** of the carriers plays a significant role in the magnetofingerprint. We next describe the effect of tilting **H** at an angle θ to **c** in the y-z plane. Figure 4(a) shows plots of the conductance vs H in sample $G4$ at selected θ, with T fixed at 2.2 K. At each θ, the curve is comprised of the weak-field quantum anomaly superimposed on a parabolic (semiclassical) background. At $\theta = 85°$, the orbital term is negligible compared with the spin term because the flux inside the sample is reduced by a factor of 40. Hence the anomaly may be identified with the spin degrees alone.

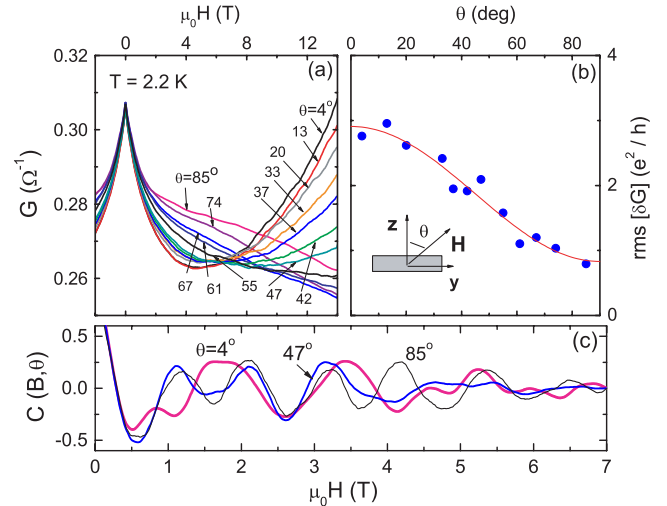As in Fig. 3, we have extracted the conductance fluctuations at each θ. The gradual decrease of the amplitude

FIG. 4 (color online). The magnetofingerprint signal in tilted field. Panel (a) shows the MR curves in $G4$ at selected field-tilt angles $4° < \theta < 85°$ at $T = 2.2$ K. Panel (b) shows the rms amplitude rms[δG] vs tilt angle θ (θ is defined in inset). The fit to rms[δG] $= [a + b\cos^2(\theta)](e^2/h)$ yields $a = 0.832$ and $b = 2.08$ (solid curve). Panel (c) plots the correlation function $\mathcal{C}(B)$ vs H at selected θ.

rms$[\delta G]$ vs θ fits well to $[a + b\cos^2\theta]e^2/h$ [Fig. 4(b)]. The first term a represents the spin term, while the second term ($\sim H_z^2$) is from orbital coupling. At maximum tilt (85°), only the spin term a (comprising 29% of the rms) survives. This is a rare example of a conductor in which the spin degrees are shown to generate a fingerprint signal. The correlation function $\mathcal{C}(B, \theta)$ of the fluctuations [shown in panel (c)] remains oscillatory with the same field period $B_p \sim 1$ T at all θ.

As displayed in Figs. 2(a) and 2(b), the weak-field anomaly in the MR has a ln$H$ dependence that may be expressed as

$$\Delta G(H) = -\frac{e^2}{h}[A_{\mathrm{orb}} + A_{\mathrm{spin}}]\ln H, \qquad (2)$$

where A_{orb} and A_{spin} (the orbital and spin terms, respectively) are both positive and comparable in magnitude. A positive A_{orb} implies field suppresion of antilocalization in a 2D (two-dimensional) system (theory [22] predicts $A_{\mathrm{orb}} = 1/2\pi$). In 2D systems, Coulomb interaction effects lead to a spin-Zeeman term of the form in Eq. (2) with $A_{\mathrm{spin}} = \tilde{F}_\sigma/2\pi$, where the parameter $\tilde{F}_\sigma$ is of order 1 [23]. However, despite the suggestive ln$H$ dependence, we again encounter a large discrepancy in the size of the anomaly. The fit in Fig. 2(b) yields $A_{\mathrm{orb}} = 122$ and $A_{\mathrm{spin}} = 78$ for $G4$. Both are 500–700× larger than the theoretical 2D values (see Table I).

The most interesting question raised by these results concerns the nature of the states in the gap responsible for the magnetofingerprint signal in nonmetallic Bi_2Se_3. Interpreting G in $G4$ as a 2D sheet conductance would give $G/(e^2/h) = k_F\ell \sim 8000$, which is far too large compared with $k_F\ell \sim 120$ given by S_F measured in the metallic crystals. This implies that the in-gap states in $G3$–$G8$ are bulklike. On the other hand, the log$H$ antilocalization anomaly identified in Eq. (2) implies that they have 2D character (despite the large A_{orb} and A_{spin}). We remark that there is evidence that ties the bulk in-gap states to the SS in Bi_2Se_3. In the ARPES results, bulk states with 2D dispersion are seen to coexist with SS throughout the gap region [shown in yellow in Figs. 1(a) and 1(b) of Xia et al. [8]]. They propose that the bulk states are confined by band bending near the surface. If hybridization with the SS is strong, we expect that the bulk states will also display a large Rashba coupling that locks the spin transverse to **k**, thereby explaining the role played by the spins. If the 2D bulk gap states share the unusual properties of the SS, the long-range phase-coherent nature of the fingerprint signal may be traced ultimately to the protected nature of the SS.

The anomalies reported here provide a window into the unusual transport properties of the SS.

[1] L. Fu, C. L. Kane, and E. J. Mele, Phys. Rev. Lett. **98**, 106803 (2007).
[2] J. E. Moore and L. Balents, Phys. Rev. B **75**, 121306(R) (2007).
[3] B. A. Bernevig and S. C. Zhang, Phys. Rev. Lett. **96**, 106802 (2006).
[4] B. A. Bernevig, T. Hughes, and S. C. Zhang, Science **314**, 1757 (2006).
[5] L. Fu and C. L. Kane, Phys. Rev. B **76**, 045302 (2007).
[6] D. Hsieh et al., Nature (London) **452**, 970 (2008).
[7] D. Hsieh et al., Science **323**, 919 (2009).
[8] Y. Xia et al., Nature Phys. **5**, 398 (2009).
[9] D. Hsieh et al., Nature (London) **460**, 1101 (2009).
[10] Y. L. Chen et al., Science **325**, 178 (2009).
[11] P. A. Lee, A. D. Stone, and H. Fukuyama, Phys. Rev. B **35**, 1039 (1987).
[12] Y. S. Hor et al., Phys. Rev. B **79**, 195208 (2009).
[13] B. L. Al'tshuler, A. G. Aronov, and B. Z. Spivak, Pis'ma Zh. Eksp. Teor. Fiz. **33**, 101 (1981) [JETP Lett. **33**, 94 (1981)].
[14] D. Y. Sharvin and Y. V. Sharvin, JETP Lett. **34**, 272 (1981).
[15] C. P. Umbach, C. Van Haesendonck, R. B. Laibowitz, S. Washburn, and R. A. Webb, Phys. Rev. Lett. **56**, 386 (1986).
[16] B. Pannetier, J. Chaussy, R. Rammal, and P. Gandit, Phys. Rev. Lett. **53**, 718 (1984).
[17] R. A. Webb, S. Washburn, C. P. Umbach, and R. B. Laibowitz, Phys. Rev. Lett. **54**, 2696 (1985); S. Washburn, C. P. Umbach, R. B. Laibowitz, and R. A. Webb, Phys. Rev. B **32**, 4789 (1985).
[18] V. Chandrasekhar, M. J. Rooks, S. Wind, and D. E. Prober, Phys. Rev. Lett. **55**, 1610 (1985).
[19] A. D. Stone, Phys. Rev. Lett. **54**, 2692 (1985).
[20] B. L. Al'tshuler, JETP Lett. **41**, 648 (1985).
[21] P. A. Lee and A. D. Stone, Phys. Rev. Lett. **55**, 1622 (1985).
[22] S. Hikami, A. I. Larkin, and Y. Nagaoka, Prog. Theor. Phys. **63**, 707 (1980).
[23] P. A. Lee and T. V. Ramakrishnan, Rev. Mod. Phys. **57**, 287 (1985).